

ON DISCRETE RAREFACTION WAVES IN AN NLS TOY MODEL FOR WEAK TURBULENCE

SEBASTIAN HERR AND JEREMY L. MARZUOLA

ABSTRACT. Recently, a model Hamiltonian dynamical system has been derived to study frequency cascades in the cubic defocusing nonlinear Schrödinger equation on the torus. Here, we explore certain rarefaction wave-like solutions to this toy model which transfer mass from low to high modes.

1. INTRODUCTION

In [8] the authors Colliander-Keel-Staffilani-Takaoka-Tao studied the $2d$ defocusing cubic toroidal nonlinear Schrödinger equation,

$$(1) \quad iu_t + \Delta u - |u|^2 u = 0, \quad u(0, x) = u_0(x) \text{ for } x \in \mathbb{T}^2,$$

by developing their “Toy Model System” given by the equation

$$(2) \quad -i\partial_t b_j(t) = -|b_j(t)|^2 b_j(t) + 2b_{j-1}^2 \bar{b}_j(t) + 2b_{j+1}^2 \bar{b}_j(t), \quad \text{for } j = 1 \dots N$$

with “boundary conditions”

$$(3) \quad b_0(t) = b_{N+1}(t) = 0.$$

The b_j approximate the mass associated with families of resonantly interacting frequencies. In [9, Section 5], the authors derive a discrete Burgers type equation with a phase drag term (see (9), (10) below) and study its numerical stability within (2).

The goal of this paper is to show that a discrete rarefaction wave associated to the Burgers equation can be used to initiate interesting dynamics in (2). In particular, the aim is to prove that this mechanism transfers mass from low to high frequency nodes on a short time scale. In addition, while much of the global structure of the rarefaction wave-like solutions in (2) remains challenging to describe fully, we present several computations that give insight into the longer time behavior of discrete rarefaction wave solutions as observed in [9] and are consistent with further mass transfer.

The main goal of developing (2) in [8] is the construction of a solution to (2) which transfers mass from low index j to high j . In other words, the goal is to robustly construct frequency cascades to show that, as

stated in [9], “dispersive equations posed on tori have weakly turbulent dynamics; while there may be no finite time singularity, arbitrarily high index Sobolev norms can grow to be arbitrarily large, but finite, in finite time.” We note that here we are focusing on the dynamical system in (2) and attempting to ascertain how robust the rarefaction wave structure is under the “phase drag” inherent to dispersive Schrödinger models and the Toy Model in particular. For other works related to frequency cascades and the study of weak turbulence for NLS, we refer the reader to [4, 3, 5, 6] as well as the interesting and recent works [7, 17, 16, 22, 25, 14, 13, 15, 19, 10, 18].

The paper will proceed as follows. In Section 2, we recall some conserved quantities related to the Toy Model to be applied later. Then, in Section 3, we recall the modified discrete Burgers equation and corresponding rarefaction wave approximation using the Madelung transformation from [9]. We proceed in Section 4 to discuss properties of rarefaction wave solutions to a discrete Burgers equation, drawing largely from an explicit solution in [1, 2], and study boundary effects in symmetric discrete Burgers equation. In Section 5 we prove an error bound for the discrete Burgers rarefaction wave in (2) rigorously (and arguably sharply) using a Gronwall type argument. Finally, in Section 6, we present flux computations related to truncated conservation laws, discuss future work, open problems and an illustrative computation about the rarefaction wave linearization in discrete L^2 spaces, which we hope will provide for more robust control of mass transfer through rarefaction waves in the Toy Model.

2. CONSERVED QUANTITIES

As they will be quite useful in our studies below, we recall here the results from [8, Section 3], where the Toy Model is studied as a Hamiltonian dynamical system. The Hamiltonian is given by

$$(4) \quad H[\mathbf{b}] = \sum_{j=1}^{\infty} \left(\frac{1}{2} |b_j|^4 - 2\Re(\bar{b}_j^2 b_{j-1}^2) \right)$$

and symplectic structure,

$$(5) \quad i \frac{db_j}{dt} = \frac{\partial H[\mathbf{b}]}{\partial \bar{b}_j}, \quad j \in \mathbb{N}.$$

The model (2) admits many of the symmetries of (1), including phase invariance, scaling, time translation and time reversal. However, many of these symmetries are redundant, and the known only invariant, other

than (4), is the mass quantity

$$(6) \quad M[\mathbf{b}] = \sum_{j=1}^{\infty} |b_j|^2.$$

Using the structure of the equations, it can be seen that given $b(0)$ initially compactly supported (on a finite number of nodes), the solution $b(t)$ remains compactly supported for all time. While we are summing over all nodes above to observe conservation of H and M , as the equation with boundary conditions (3) remains compactly supported on the same region, both H and M are still conserved when one sums only from $j = 1$ to N .

Defining circles \mathbb{T}_j for $j = 1, \dots, N$ as

$$\mathbb{T}_j = \{\mathbf{b} = (b_1, \dots, b_N) \mid |\mathbf{b}|^2 = 1, |b_j| = 1, b_k = 0 \text{ for all } k \neq j\},$$

the authors in [8] point out that the flow of (2), which is referred to as $S(t)b_0$, leaves each \mathbb{T}_j invariant. In [9], it was observed that (2) also has a natural probabilistic formulation and can be seen to have some basic recurrence properties.

3. DISCRETE RAREFACTION WAVES AND THE DISCRETE BURGERS EQUATION

In this section, we recall the main aspects of [9, Section 5]. First, we make the Madelung transformation given by

$$(7) \quad b_j(t) = \sqrt{\rho_j} e^{i\phi_j(t)}.$$

with *out of phase* initial interactions set by $\phi_j(0) = \phi_{j-1}(0) + \frac{\pi}{4}$. Initially, the hydrodynamic equations have a Burgers type structure

$$(8) \quad \begin{cases} \dot{\phi}_j = 0 \\ \dot{\rho}_j = -4\rho_j\rho_{j-1} - 4\rho_j\rho_{j+1} = -8\rho_j \left(\frac{\rho_{j+1} - \rho_{j-1}}{2}\right). \end{cases}$$

This system has beautiful discrete rarefaction waves propagating towards infinity and a backwards dispersive shock. We also refer the reader to [20] for another example of a discrete conservation law with a dispersive shock, cf. Subsection 6.3. We call this the discrete Burgers equation since in the continuum limit we would have

$$\rho_t = -8\rho\nabla\rho,$$

which, with initial data

$$\rho(0, x) = \begin{cases} 0 & x \leq 0, \\ 1 & 0 < x < \infty, \end{cases}$$

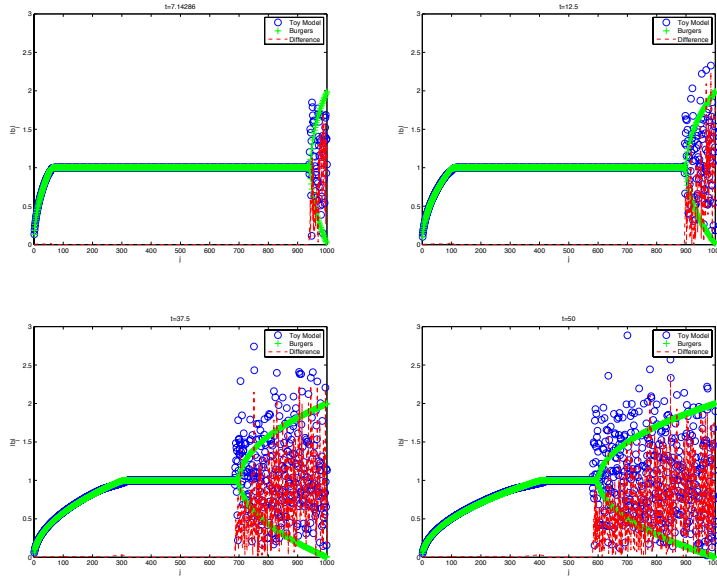


FIGURE 1. A comparison of the Toy Model and the symmetric discrete Burgers rarefaction waves.

has the known rarefaction wave solution

$$\rho(t, x) = \begin{cases} 0 & x < 0, \\ \frac{x}{8t} & 0 < x < 8t, \\ 1 & 8t < x. \end{cases}$$

However, in our discrete system, there is drag in the phase coefficients that does not allow us to permanently assume an out of phase framework:

$$(9) \quad \dot{\phi}_j = -\rho_j + 2\rho_{j-1} \cos(2(\phi_{j-1} - \phi_j)) + 2\rho_{j+1} \cos(2(\phi_{j+1} - \phi_j)),$$

$$(10) \quad \dot{\rho}_j = -4\rho_j \rho_{j-1} \sin(2(\phi_{j-1} - \phi_j)) - 4\rho_j \rho_{j+1} \sin(2(\phi_{j+1} - \phi_j)).$$

Let us recall some numerical simulations from [9] to motivate our analysis below. There, it is numerically studied how solutions evolve, with the initial condition

$$(11) \quad b_j = \exp i \{(j-1)\pi/4\}.$$

In Figure 1 we show the numerically computed time evolution of the Toy Model compared to that of a backward discrete Burgers equation.

4. ANALYSIS OF THE RAREFACTION WAVE

In this section, we present some analytic results on the rarefaction wave. In particular, we compare solutions to the discrete Toy Model

in the hydrodynamic formulation to computations from an explicit solution to a discrete Burgers Equation, which behaves comparably to a continuous Burgers equation.

4.1. Alternative Coordinates. Since the drag term in the phase (the term $-\rho_j$ in (9) and $-i|b_j|^2 b_j$ in (2)) introduces errors in the Burgers evolution, we introduce the coordinate $\theta_j = \phi_j - \phi_{j-1}$. In the new coordinates, we have

$$(12) \quad \dot{\theta}_j = -(\rho_j - \rho_{j-1}) - 2(\rho_j - \rho_{j-1}) \cos(2\theta_j) \\ + 2\rho_{j+1} \cos(2\theta_{j+1}) - 2\rho_{j-2} \cos(2\theta_{j-1}),$$

$$(13) \quad \dot{\rho}_j = 4\rho_j \rho_{j-1} \sin(2\theta_j) - 4\rho_j \rho_{j+1} \sin(2\theta_{j+1}).$$

4.2. Scaling Discrete Burgers. We wish to use an exact solution to a discrete Burgers equation in order to establish an envelope solution to the Toy Model. The envelope solution we wish to follow is for the symmetric Burgers equation

$$(14) \quad \dot{\tilde{\rho}}_j = -\tilde{\rho}_j (\tilde{\rho}_{j+1} - \tilde{\rho}_{j-1}).$$

It is possible to solve such an equation using inverse scattering (see [12, 11, 21] as we will discuss later in Section 7), but a priori bounds on the amplitude then become less clear than is desirable for comparison with the Toy Model. The best treatment of which we have found in the works [1, 2], where for the backward discrete Burgers

$$(15) \quad \dot{p}_j = -p_j (p_j - p_{j-1}),$$

an explicit solution is derived. To do so, they introduce the transformation $p_j = \frac{a_j}{a_{j+1}}$, and the problem is converted to the recursively solved linear system of ODEs

$$\dot{a}_j = a_{j-1}.$$

With initial data configured only for a rarefaction wave solution

$$(16) \quad p_j(0) = \begin{cases} 0 & j \leq 0, \\ 1 & 1 \leq j < \infty, \end{cases}$$

this has a solution of the form

$$a_j(t) = (1 + t + \dots + \frac{1}{(j-1)!} t^{j-1}).$$

Note, this solution does not have finite speed of propagation, in that every non-zero q_j will change for all $t > 0$, not just those to the left

of a front as in the continuous shock solution. However, the resulting solution in (15) is

$$\begin{aligned} p_j(t) &= \frac{1 + t + \cdots + \frac{1}{(j-1)!}t^{j-1}}{1 + t + \cdots + \frac{1}{(j)!}t^j} = 1 - \frac{\frac{1}{(j)!}t^j}{1 + t + \cdots + \frac{1}{(j)!}t^j} \\ &= 1 - \frac{1}{(j)!}t^j + h.o.t. \end{aligned}$$

for short times t . Then, to solve the rescaled Burgers equation

$$(17) \quad \dot{p}_j(\alpha, \beta, t) = -\alpha p_j(p_j - p_{j-1}), \quad p_j(\alpha, \beta, 0) = \begin{cases} 0 & j \leq 0, \\ \beta & 0 < j < \infty, \end{cases}$$

we have

$$p_j(t) = \beta \frac{1 + \alpha\beta t + \cdots + \frac{1}{(j-1)!}(\alpha\beta t)^{j-1}}{1 + \alpha\beta t + \cdots + \frac{1}{(j)!}(\alpha\beta t)^j}.$$

Generally, in order to control both the dispersive shock¹ created by a large jump near $j = N$ and the phase splitting mechanism at large amplitude for lattice sites near $j = 1$, the parameter β will be set by us to simply be $\epsilon/8$ to study rarefaction waves in the Toy Model, where the 8 is a scaling parameter chosen for convenience. Indeed, due to the scalings above and the nature of the Toy Model, we study the following “backwards” discrete Burgers equation,

$$(18) \quad \dot{p}_j = -8p_j(p_j - p_{j-1}).$$

We have via the remarkable explicit solution from [1, 2], the rescaled solution

$$(19) \quad \begin{aligned} p_j &= \frac{\epsilon}{8} \frac{1 + (\epsilon t) + \cdots + \frac{1}{(j-1)!}(\epsilon t)^{j-1}}{1 + (\epsilon t) + \cdots + \frac{1}{(j)!}(\epsilon t)^j} \\ &= \frac{1}{8} \frac{\partial_t(1 + (\epsilon t) + \cdots + \frac{1}{(j)!}(\epsilon t)^j)}{1 + (\epsilon t) + \cdots + \frac{1}{(j)!}(\epsilon t)^j}. \end{aligned}$$

While we make use of this rescaling in order to get natural smallness in the phase drift term, we can always rescale the solution back to order 1 by the same argument, see Remark 4.2 for a further discussion.

Now, as a leading order description of the behavior in the full Toy Model, we propose the following modified discrete Burgers equation for

¹In discussions with Mark Hoefer, he has suggested that this backward propagating wave takes on more features of turbulence than of a dispersive shock front. However, to investigate this involves connecting the oscillations from the front of the backward propagating front in a more robust fashion.

capturing the dynamics.

$$(20) \quad \begin{cases} \dot{\tilde{\theta}}_j = -(\tilde{\rho}_j - \tilde{\rho}_{j-1}) \\ \dot{\tilde{\rho}}_j = \tilde{\rho}_j \tilde{\rho}_{j+1} - 4\tilde{\rho}_j \tilde{\rho}_j = -4\tilde{\rho}_j (\tilde{\rho}_{j+1} - \tilde{\rho}_{j-1}). \end{cases}$$

Note that these equations are completely decoupled.

We will show in our analysis of (2) in Section 5 that errors arising around this approximation are small on the time scales we study. It is however the errors in phase term that account primarily for the slight deviations from the pure rarefaction wave on the left and the approximation of discrete symmetric Burgers by discrete backwards Burgers on the right in Figure 1.

4.3. A Priori Estimates for Rarefaction Waves. In this section, we want to prove a priori bounds on the evolution of (20) based upon a leading order approximation using (15). We focus on the amplitude equations. Specifically, we will approximate solutions to

$$\dot{\tilde{\rho}}_j = -4\tilde{\rho}_j(\tilde{\rho}_{j+1} - \tilde{\rho}_{j-1}) \quad \tilde{\rho}_j(0) = \epsilon/8 \text{ for } j = 1, \dots, N,$$

by the explicit rarefaction wave solution defined in (19) to

$$(21) \quad \dot{p}_j = -8p_j(p_j - p_{j-1}), \quad p_j(0) = \epsilon/8 \text{ for } j = 1, \dots, N.$$

Setting $q_j = \tilde{\rho}_j - p_j$ and $\sigma_j = p_{j+1} - p_j$, we observe

$$(22) \quad \begin{aligned} \dot{q}_j &= -4p_j(\sigma_j - \sigma_{j-1}) - 4q_j(\sigma_j + \sigma_{j-1}) \\ &\quad - 4p_j(q_{j+1} - q_{j-1}) - 4q_j(q_{j+1} - q_{j-1}), \\ q_j(0) &= 0. \end{aligned}$$

Let us define the forcing component of this system of ODEs as

$$F_j = -4p_j(\sigma_j - \sigma_{j-1}).$$

Moving the term $4q_j(\sigma_j + \sigma_{j+1})$ to the left hand side and applying an integrating factor argument, we obtain

$$(23) \quad |q_j|(t) \leq \int_0^t e^{-4 \int_s^t (\sigma_j + \sigma_{j-1})(s') ds'} (|F_j| + 8\|q\|_\infty |p_j| + 8\|q\|_\infty |q_j|) ds$$

uniformly on the time interval $[0, \epsilon^{-1}\delta]$. Here and in the sequel we use the notation $\|q\|_\infty := \sup_{0 \leq t \leq T} \sup_{j \in \mathbb{Z}} |q_j(t)|$.

The following lemma contains the a priori estimate for $\|q\|_\infty$.

Lemma 4.1. *Fix $\delta < 1/8$. For all $0 < \epsilon \leq \delta$ and $T = \epsilon^{-1}\delta$ and q_j, p_j as in (21), (22) respectively, we have*

$$(24) \quad \|q\|_\infty \leq \frac{\epsilon\delta}{2}.$$

Proof. The proof follows by a simple bootstrap argument on (23). Let us note that the exponential factor is uniformly bounded by 1 for every j except at $j = N$ where it is bounded by e^δ on our time scale. Then, from the bootstrapping assumption we obtain

$$\|q\|_\infty \leq e^\delta \left(16 \frac{\epsilon^2}{8^2} T + \epsilon^2 \delta T / 2 + 2\epsilon^2 \delta^2 T \right),$$

which is bounded above by

$$\frac{\epsilon\delta}{2} \left(e^\delta \left[\frac{1}{2} + \frac{\delta}{2} + 4\epsilon\delta^2 \right] \right) < \frac{\epsilon\delta}{2}$$

for any $\delta < 1/8$, provided $\epsilon \leq \delta$. \square

Armed with this a priori estimate, we can get refined estimates for $|q_j(t)|$ for $0 \leq j \leq N - 1$ using the fact that the exponential factor is bounded by 1 in these cases. Indeed, a direct calculation using the explicit solution on time scale T shows that for instance $|F_1| < \epsilon^2/8^2(1 - \epsilon t)^2$. In turn, we can show

$$|q_1(t)| \leq \epsilon\delta \left(\frac{1}{2^4} + \delta + 8\delta^2 \right) < \frac{\epsilon\delta}{12}$$

for δ chosen sufficiently small. Even stronger estimates hold for $0 < j < N$.

A symmetric argument using the (22) for q_N shows that

$$|q_N(T)| \geq \frac{\epsilon\delta}{16},$$

by recognizing that $F_N \approx 4\rho_N^2$ and $\sigma_N = 4p_{N-1}$. We will show in Section 4.4 from a different argument that ρ_N is increasing in fact, but without such quantitative bounds as we are able to gain from (22).

Remark 4.2. *By nature of the construction, we now have that*

$$\rho_0(t) \leq p_j(t) + \left(\frac{\epsilon\delta}{12} \right).$$

Hence, near the end of our evolution the rarefaction wave at the left of the grid has size roughly

$$p_0(T) = \frac{\epsilon}{8} \frac{1}{1 + \epsilon T} \approx \frac{\epsilon}{8} (1 - \delta),$$

which is less than the initial amplitude $\epsilon/8$ even when compared to the error. Hence, we observe that what we have seen in Figures 1, namely that the rarefaction wave solution moves mass to the right initially in symmetric Burgers. Similar estimates can be proven using the stronger bounds on q_j for $j > 1$, though on the time scale T most nodes have

moved very little. While we are not arguing this makes the rarefaction wave solution a good approximation for long times, we can observe both that the rarefaction wave initializes a motion of mass towards the right for the low modes. Numerically, we observe that the rarefaction wave behavior is much more robust than we can fully understand at the moment.

4.4. The Shock vs. Rarefaction in the Toy Model. Let us analyze the symmetric discrete Burgers equation in (8) with initial condition

$$(25) \quad \tilde{\rho}_j = 1 \text{ for } 1 \leq j \leq 2N, \quad \tilde{\rho}_j = 0 \text{ otherwise.}$$

Then, we observe that such an equation can be decomposed into a coupled system of equations for $s_j = \tilde{\rho}_{2j}$ and $r_j = \tilde{\rho}_{2j+1}$, which results in the system

$$\dot{s}_j = -4s_j(r_j - r_{j-1}), \quad \dot{r}_j = -4r_j(s_{j+1} - s_j).$$

Now, if we look at the right-most points, we observe

$$\dot{s}_N = 4s_N(r_{N-1}), \quad \dot{r}_{N-1} = -4r_{N-1}(s_N - s_{N-1}),$$

which given that $r_j, s_j > 0$ for $1 \leq j \leq N$ implies that s_N is an increasing function. As a result, this implies that r_{N-1} is a decreasing function. Propagating this down the line interactions, we observe that the symmetric Burgers causes a splitting from the right endpoint instead of a shock moving right, see Figure 2 for a numerical simulation of this effect. Note that the leading order component on the left is still that of a rarefaction wave however. It is indeed this wave front we believe acts as the envelope for the Toy Model rarefaction wave, however as we do not have explicit control on its evolution, we focus on the rarefaction wave coming from the appropriate backwards Burgers evolution as in (15).

5. PERTURBATION THEORY

5.1. Equations for error terms. Let us now fix a lattice with N nodes and explicitly study equations (12) and (13) with initial conditions given by

$$(26) \quad \theta_j(0) = \frac{\pi}{4}, \quad \rho_j(0) = \frac{\epsilon}{8}$$

for all $j = 1, \dots, N$, and 0 otherwise.

We wish to observe what sorts of error terms arise when we perturb around the dynamics in (20) in the full Toy Model. To do this, we will first derive a new solution for (14) as a perturbation of the explicit solutions explored above for (15) in Section 4.2.

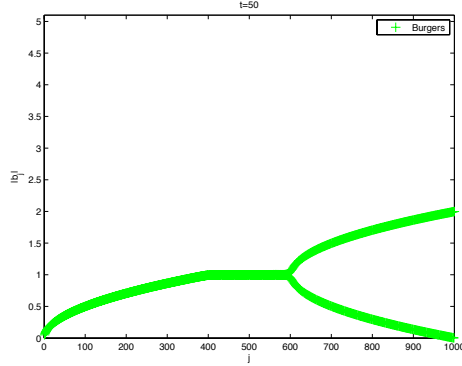


FIGURE 2. The left moving split that generates the dispersive shock from the symmetric Burgers evolution of (25). This has been evolved to time $T = 50.0$ on a lattice of size $N = 1000$.

The difficulty here with directly using (20) is that we must first approximate the existence of a rarefaction wave like solution and prove a priori estimates. However, we can study the evolution of

$$\hat{\theta}_j = \theta_j - \tilde{\theta}_j, \quad \hat{\rho}_j = \rho_j - \tilde{\rho}_j$$

by linearizing the sin and cos terms in (12), (13). Before we proceed, recall the expansions

$$(27) \quad \sin(\pi/2 + x) = 1 - \frac{x^2}{2!} - \dots, \quad \cos(\pi/2 + x) = x - \frac{x^3}{3!} + \dots$$

Let us define

$$(28) \quad -\tilde{\gamma}_j = \int_0^t (\tilde{\rho}_j - \tilde{\rho}_{j-1}) ds.$$

Note that there are much stronger and j dependent bounds on the components stemming from the exact solution $\vec{p}(t)$,

$$\begin{aligned} \int_0^t (p_j - p_{j-1}) ds &= \frac{1}{8} \log \left(\frac{1 + \epsilon t + \dots + \frac{1}{(j)!} (\epsilon t)^j}{(1 + \epsilon t + \dots + \frac{1}{(j-1)!} (\epsilon t)^{j-1})} \right) \\ &= \frac{1}{8} \log \left(1 + \frac{\frac{1}{(j)!} (\epsilon t)^j}{(1 + \epsilon t + \dots + \frac{1}{(j-1)!} (\epsilon t)^{j-1})} \right) \\ &\leq \frac{1}{8} \log(1 + \frac{\epsilon t}{j}) \leq \frac{\epsilon t}{8j} \quad \text{if } \epsilon t \leq 1. \end{aligned}$$

Then using $T = \delta\epsilon^{-1}$ and the corresponding bounds we have from Section 4.3, one has the crude bound

$$(29) \quad |\tilde{\gamma}_j| \leq \frac{\delta}{8} + 2T \frac{\epsilon\delta}{2} \leq \frac{\delta}{8} + \delta^2.$$

Similarly, we define

$$(30) \quad \tilde{\sigma}_j = (\tilde{\rho}_j - \tilde{\rho}_{j-1}),$$

which then using the explicit properties of $\vec{p}(t)$ and bounds we have from Section 4.3, we have the crude bound

$$(31) \quad |\tilde{\sigma}_j| \leq \frac{\epsilon}{8(j-1)!} + \epsilon\delta.$$

These definitions will allow us to simplify the process of collecting (generically small in amplitude) components of our expansion.

By linearizing \cos in (12), we observe that

$$\begin{aligned} \dot{\hat{\theta}}_j &= -(\hat{\rho}_j - \hat{\rho}_{j-1})(1 + 2\cos(\pi/2 + 2(\hat{\theta}_j + \tilde{\gamma}_j))) \\ &\quad - 2(\tilde{\rho}_j - \tilde{\rho}_{j-1})\cos(\pi/2 + 2(\hat{\theta}_j + \tilde{\gamma}_j)) \\ &\quad + 2(\hat{\rho}_{j+1} + \tilde{\rho}_{j+1})\cos(\pi/2 + 2(\hat{\theta}_{j+1} + \tilde{\gamma}_{j+1})) \\ &\quad - 2(\hat{\rho}_{j-2} + \tilde{\rho}_{j-2})\cos(\pi/2 + 2(\hat{\theta}_{j-1} + \tilde{\gamma}_{j-1})) \\ &= -(\hat{\rho}_j - \hat{\rho}_{j-1}) + 4[(\tilde{\rho}_j - \tilde{\rho}_{j-1}) + (\hat{\rho}_j - \hat{\rho}_{j-1})](\tilde{\gamma}_j + \hat{\theta}_j) \\ &\quad - 4(\tilde{\rho}_{j+1} + \hat{\rho}_{j+1})(\tilde{\gamma}_{j+1} + \hat{\theta}_{j+1}) + 4(\tilde{\rho}_{j-2} + \hat{\rho}_{j-2})(\tilde{\gamma}_{j-1} + \hat{\theta}_{j-1}) \\ &\quad + \tilde{E}_{1,j}(\hat{\theta} + \tilde{\gamma}, \hat{\rho}), \end{aligned}$$

provided that $\hat{\sigma}_j = \hat{\rho}_j - \hat{\rho}_{j-1}$ and

$$\begin{aligned} \tilde{E}_{1,j}(\hat{\theta} + \tilde{\gamma}, \hat{\rho}) &= -2\hat{\sigma}_j[\cos(\pi/2 + 2(\hat{\theta}_j + \tilde{\gamma}_j)) + 2(\hat{\theta}_j + \tilde{\gamma}_j)] \\ &\quad - 2\tilde{\sigma}_j[\cos(\pi/2 + 2(\hat{\theta}_j + \tilde{\gamma}_j)) + 2(\hat{\theta}_j + \tilde{\gamma}_j)] \\ &\quad + 2(\hat{\rho}_{j+1} + \tilde{\rho}_{j+1})[\cos(\pi/2 + 2(\hat{\theta}_{j+1} + \tilde{\gamma}_{j+1})) + 2(\hat{\theta}_{j+1} + \tilde{\gamma}_{j+1})] \\ &\quad - 2(\hat{\rho}_{j-2} + \tilde{\rho}_{j-2})[\cos(\pi/2 + 2(\hat{\theta}_{j-1} + \tilde{\gamma}_{j-1})) + 2(\hat{\theta}_{j-1} + \tilde{\gamma}_{j-1})]. \end{aligned}$$

Defining

$$E_{1,j}(\hat{\theta} + \tilde{\gamma}, \hat{\rho}) = 4(\hat{\rho}_j - \hat{\rho}_{j-1})\hat{\theta}_j - 4\hat{\rho}_{j+1}\hat{\theta}_{j+1} + 4\hat{\rho}_{j-2}\hat{\theta}_{j-1} + \tilde{E}_{1,j}(\hat{\theta} + \tilde{\gamma}, \hat{\rho}),$$

we obtain

$$(32) \quad \begin{aligned} \dot{\hat{\theta}}_j &= -(\hat{\rho}_j - \hat{\rho}_{j-1})(1 - 4\tilde{\gamma}_j) + 4(\tilde{\rho}_j - \tilde{\rho}_{j-1})\hat{\theta}_j \\ &\quad - 4\tilde{\gamma}_{j+1}\hat{\rho}_{j+1} - 4\tilde{\rho}_{j+1}\hat{\theta}_{j+1} + 4\tilde{\gamma}_{j-1}\hat{\rho}_{j-2} + 4\tilde{\rho}_{j-2}\hat{\theta}_{j-1} \\ &\quad + f_{1,j}(t) + E_{1,j}(\hat{\theta} + \tilde{\gamma}, \hat{\rho}), \end{aligned}$$

where

$$\begin{aligned} f_{1,j}(t) &= 4\tilde{\sigma}_j\tilde{\gamma}_j - 4(\tilde{\rho}_{j+1}\tilde{\gamma}_{j+1} - \tilde{\rho}_{j-2}\tilde{\gamma}_{j-1}) \\ &= 4\tilde{\sigma}_j\tilde{\gamma}_j - 4\tilde{\rho}_{j+1}(\tilde{\gamma}_{j+1} - \tilde{\gamma}_{j-1}) - 4\tilde{\gamma}_{j-1}(\tilde{\rho}_{j+1} - \tilde{\rho}_{j-2}). \end{aligned}$$

Similarly, by linearizing \sin in (13) we obtain

$$\begin{aligned} \dot{\hat{\rho}}_j &= -4(\hat{\rho}_j + \tilde{\rho}_j)(\hat{\rho}_{j+1} + \tilde{\rho}_{j+1})\sin(\pi/2 + 2(\hat{\theta}_{j+1} + \tilde{\gamma}_{j+1})) \\ &\quad + 4(\hat{\rho}_j + \tilde{\rho}_j)(\hat{\rho}_{j-1} + \tilde{\rho}_{j-1})\sin(\pi/2 + 2(\hat{\theta}_j + \tilde{\gamma}_j)) \\ &\quad + 8\tilde{\rho}_j(\tilde{\rho}_j - \tilde{\rho}_{j-1}) \\ (33) \quad &= -4\hat{\rho}_j(\tilde{\rho}_{j+1} - \tilde{\rho}_{j-1}) - 4\tilde{\rho}_j\hat{\rho}_{j+1} + 4\tilde{\rho}_j\hat{\rho}_{j-1} \\ &\quad + E_{2,j}(\hat{\theta} + \tilde{\gamma}, \hat{\rho}), \end{aligned}$$

using

$$\begin{aligned} \tilde{E}_{2,j}(\hat{\theta} + \tilde{\gamma}, \hat{\rho}) &= -4(\hat{\rho}_j + \tilde{\rho}_j)(\hat{\rho}_{j+1} + \tilde{\rho}_{j+1})[\sin(\pi/2 + 2(\hat{\theta}_{j+1} + \tilde{\gamma}_{j+1})) - 1] \\ &\quad + 4(\hat{\rho}_j + \tilde{\rho}_j)(\hat{\rho}_{j-1} + \tilde{\rho}_{j-1})[\sin(\pi/2 + 2(\hat{\theta}_j + \tilde{\gamma}_j)) - 1] \end{aligned}$$

and

$$E_{2,j}(\hat{\theta} + \tilde{\gamma}, \hat{\rho}) = 4\hat{\rho}_j\hat{\rho}_{j-1} - 4\hat{\rho}_j\hat{\rho}_{j+1} + \tilde{E}_{2,j}(\hat{\theta} + \tilde{\gamma}, \hat{\rho}).$$

At this stage, we set out to explore in what sense a rarefaction wave-like solution from the backward Burgers equation approximates the solution to

$$\begin{aligned} \dot{\theta}_j &= -(\rho_j - \rho_{j-1}) - 2(\rho_j - \rho_{j-1})\cos(2\theta_j) \\ &\quad + 2\rho_{j+1}\cos(2\theta_{j+1}) - 2\rho_{j-2}\cos(2\theta_{j-1}), \\ \dot{\rho}_j &= 4\rho_j\rho_{j-1}\sin(2\theta_j) - 4\rho_j\rho_{j+1}\sin(2\theta_{j+1}). \end{aligned}$$

with initial data

$$\theta_j(0) = \frac{\pi}{4}, \quad \rho_j(0) = \frac{\epsilon}{8}$$

for all $j = 1, \dots, N$, and 0 otherwise.

5.2. A Gronwall Estimate. Multiplying (32) by $\hat{\theta}_j$ and (33) by $\hat{\rho}_j$, we obtain

$$\begin{aligned} (34) \quad &\frac{1}{2} \frac{d}{dt} \|\hat{\theta}\|_{\ell^\infty}^2 \leq 12\|\tilde{\rho}\|_{\ell^\infty} \|\hat{\theta}\|_{\ell^\infty}^2 + 8\|\tilde{\gamma}\|_{\ell^\infty} \|\hat{\rho}\|_{\ell^\infty} \|\hat{\theta}\|_{\ell^\infty} \\ &\quad + 2\|\hat{\rho}\|_{\ell^\infty} \|1 - 4\tilde{\gamma}\|_{\ell^\infty} \|\hat{\theta}\|_{\ell^\infty} + \|f_1\|_{\ell^\infty} \|\hat{\theta}\|_{\ell^\infty} + \|E_1(\hat{\theta} + \tilde{\gamma}, \hat{\rho})\|_{\ell^\infty} \|\hat{\theta}\|_{\ell^\infty}, \end{aligned}$$

$$(35) \quad \frac{1}{2} \frac{d}{dt} \|\hat{\rho}\|_{\ell^\infty}^2 \leq 12\|\tilde{\rho}\|_{\ell^\infty} \|\hat{\rho}\|_{\ell^\infty}^2 + \|E_2(\hat{\theta} + \tilde{\gamma}, \hat{\rho})\|_{\ell^\infty} \|\hat{\rho}\|_{\ell^\infty},$$

uniformly on the time interval $[0, \delta\epsilon^{-1}]$.

The following lemma contains the crucial Gronwall estimates. Applying the relations $ab \leq Ta^2 + \frac{1}{4T}b^2$ in the $\hat{\theta}$ equations and $ab \leq 2Ta^2 + \frac{1}{2T}b^2$ in the $\hat{\rho}$ equations for $T > 0$, we can write down crude bounds directly from immediate consequence of (34) and (35). On the time scale $T = \delta\epsilon^{-1}$, we have from above that

$$\tilde{\rho}_j \leq \frac{\epsilon}{8} + \frac{\epsilon\delta}{2}$$

and

$$\tilde{\gamma}_j \leq \frac{\delta}{8} + \delta^2.$$

Lemma 5.1. *For all $0 < t \leq T = \delta\epsilon^{-1}$ we have*

(36)

$$\|\hat{\theta}(t)\|_{\ell^\infty}^2 \leq C_1 e^{24 \int_0^t \|\tilde{\rho}\|_{\ell^\infty} ds} I_1(t), \quad \text{where}$$

$$\begin{aligned} I_1(t) &= \left(\int_0^t (16\|\tilde{\gamma}\|_{\ell^\infty} + 2\|1 - 4\tilde{\gamma}\|_{\ell^\infty})T\|\hat{\rho}\|_{\ell^\infty}^2 + 2T\|f_1\|_{\ell^\infty}^2 + 2T\|E_1(\hat{\theta} + \tilde{\gamma}, \hat{\rho})\|_{\ell^\infty}^2 ds \right) \\ &\leq \left(\int_0^t (2 + 3\delta + 24\delta^2)T\|\hat{\rho}\|_{\ell^\infty}^2 + 2T\|f_1\|_{\ell^\infty}^2 + 2T\|E_1(\hat{\theta} + \tilde{\gamma}, \hat{\rho})\|_{\ell^\infty}^2 ds \right), \end{aligned}$$

and

$$(37) \quad \begin{aligned} \|\hat{\rho}(t)\|_{\ell^\infty}^2 &\leq C_2 e^{24 \int_0^t \|\tilde{\rho}\|_{\ell^\infty} ds} I_2(t), \quad \text{where} \\ I_2(t) &= \left(\int_0^t T\|E_2(\hat{\theta} + \tilde{\gamma}, \hat{\rho})\|_{\ell^\infty}^2 ds \right). \end{aligned}$$

We can then bound the constants by

$$C_1 = e^{\frac{1}{2T} \int_0^t (8\|\tilde{\gamma}\|_{\ell^\infty} + \|1 - 4\tilde{\gamma}\|_{\ell^\infty} + 2) ds} \leq e^{\frac{3}{2} + \frac{3}{2}\delta + 6\delta^2} \leq 8,$$

$$C_2 = e^1 < 3,$$

and

$$2 + 3\delta + 24\delta^2 \leq 3$$

for δ sufficiently small.

5.3. Main result. We proceed with a bootstrap argument to prove uniform bounds for $(\hat{\theta}, \hat{\rho})$. We will control the error terms with respect to the parameter ϵ for a grid of size N up to a time $T = \epsilon^{-1}$.

Theorem 5.1. *There exists an $1/16 > \delta > 0$, such that for any $0 < \epsilon$ sufficiently small, $N > 0$, given initial data (26) depending upon ϵ for equations (12)-(13), the solution (θ, ρ) to (12), (13) satisfies*

$$\|\theta - \tilde{\theta}\|_{L^\infty \ell^\infty} \leq \frac{\delta}{8}, \quad \|\rho - \tilde{\rho}\|_{L^\infty \ell^\infty} \leq \frac{\delta\epsilon}{32}$$

for all $0 \leq t \leq T = \delta\epsilon^{-1}$. Here, $(\tilde{\theta}(t), \tilde{\rho}(t))$ satisfy (20) with initial data (26).

Proof. Let us take a $0 < \delta < 1/16$ to be chosen later. We define $B_r(0)$ denote the closed ball of radius r centered at 0 in $L^\infty([0, T]; \ell^\infty)$, and hence take the bootstrap assumption to be that

$$(\hat{\theta}, \hat{\rho}) \in B_{\frac{\delta}{8}}(0) \times B_{\frac{\delta\epsilon}{32}}(0)$$

for all time for a given δ to be chosen later. In other words, we will assume the following bounds

$$(38) \quad \|(\hat{\theta})\|_{L_t^\infty \ell^\infty} \leq \frac{\delta}{8}, \quad \|(\hat{\rho})\|_{L_t^\infty \ell^\infty} \leq \frac{\delta\epsilon}{32}.$$

Let us note here that similar to the computation in (29), we have

$$(39) \quad e^{24 \int_0^T \|\tilde{\rho}_j\|_{\ell^\infty}(s) ds} \leq e^{24T\epsilon(\frac{1}{8} + \frac{\delta}{2})} \leq e^{4\delta}$$

for $T \leq \delta\epsilon^{-1}$. Due to the bootstrap assumption we have for $t \leq \delta\epsilon^{-1}$ the bound

$$\max_j |\hat{\theta}_j| + |\tilde{\gamma}_j| \leq \frac{2\delta}{8} + \delta^2 \leq \frac{1}{24}$$

with δ chosen sufficiently small. Hence, using $\epsilon \ll \delta < 1$, we can write the explicit bounds

$$\begin{aligned} |E_{1,j}| &\leq 16\|\hat{\rho}\|_{L^\infty}\|\hat{\theta}\|_{L^\infty} + |\tilde{E}_{1,j}| < \frac{\epsilon\delta^2}{16} + 8\|\hat{\rho}\|_{L^\infty}\frac{4}{3}\|\hat{\theta} + \tilde{\gamma}\|_{L^\infty}^3 + 8\|\tilde{\rho}\|_{L^\infty}\frac{4}{3}\|\hat{\theta} + \tilde{\gamma}\|_{L^\infty}^3 \\ &< \frac{\epsilon\delta^2}{16} + \frac{\epsilon\delta}{3}\left(\frac{\delta}{2^2} + \delta^2\right)^3 + 8\left(\frac{\epsilon}{8} + \frac{\epsilon\delta}{2}\right)\frac{4}{3}\left(\frac{\delta}{2^2} + \delta^2\right)^3 \\ &< \frac{\epsilon\delta^2}{16} + 4\epsilon\left(\frac{\delta}{2^2} + \delta^2\right)^3 < \frac{3\epsilon\delta^2}{2^4}, \end{aligned}$$

$$\begin{aligned} |(f)_{1,j}| &\leq 16\|\tilde{\rho}\|_{L^\infty}\|\tilde{\gamma}\|_{L^\infty} < 16\left(\frac{\epsilon}{8} + \epsilon\delta\right)\left(\frac{\delta}{8} + \delta^2\right) \\ &\leq \epsilon\left(\frac{\delta}{4} + 4\delta^2 + 16\delta^3\right) \end{aligned}$$

and

$$|E_{2,j}| \leq 8\|\hat{\rho}\|_{L^\infty}^2 + |\tilde{E}_{2,j}| < \frac{\delta^2\epsilon^2}{2^7} + \frac{\epsilon^2}{4}\left(\frac{\delta}{2^2} + \delta^2\right)^2 < \frac{3\delta^2\epsilon^2}{2^7}$$

for ϵ sufficiently small. Here, we have taken the coefficients large enough to dominate algebraic contributions of each term in the expansions for $f_{1,2}$ and $E_{1,2}$ with the contribution from $\tilde{E}_{1,2}$ doubled in order to bound all higher order terms by twice the worst bound on those of lowest order. Careful control of such error terms will most definitely allow for

somewhat sharper bounds, however these terms are much lower order compared to boundary effects, so we do not work carefully to optimize them.

Thus, we deduce that there exists $C > 0$ (can be fixed uniformly in ϵ for δ small) such that

$$\begin{aligned} |\text{r.h.s. of (36)}| &\leq 8T^2\epsilon^2 \left[\frac{3}{16^2}\delta^2 + 2 \left(\frac{\delta}{4} + 4\delta^2 + 16\delta^3 \right)^2 + 2\frac{9\delta^4}{2^8} \right] \\ &\leq C\delta^4 < \frac{\delta^2}{64} \end{aligned}$$

and

$$\begin{aligned} |\text{r.h.s. of (37)}| &\leq 3T^2\epsilon^2 \left[\frac{9\delta^4\epsilon^2}{2^{14}} \right] \\ &\leq \frac{\epsilon^2\delta^2}{32^2}(2\delta^4) < \frac{\delta^2\epsilon^2}{32^2} \end{aligned}$$

for δ sufficiently small. Note that δ is chosen independently of ϵ and N . As a result, we can close the bootstrapping argument in $\hat{\theta}$ and $\hat{\rho}$ independent of our choice of lattice size N and any initial step size $\epsilon/8$. \square

Remark 5.2. *By nature of the construction, we now have that*

$$|b_j|^2(t) = \rho_j(t) \leq \tilde{\rho}_j(t) + \left(\frac{\epsilon\delta}{32} \right).$$

Hence, using the envelope estimates from Remark 4.2 for the explicit rarefaction wave in Section 4.3 and Theorem 5.1, near the end of our evolution the rarefaction wave at the left of the grid has size roughly bounded

$$|\rho_0(T)| < \frac{\epsilon}{8} - \frac{\epsilon\delta}{10},$$

which is less than the initial amplitude $\epsilon/8$ even when compared to the error. A symmetric argument using the growth of ρ_N shows that it has increased by a non-trivial amount. Hence, we observe that our method moves mass towards the right and given that the symmetric Burgers solution increases at the right endpoint, the Toy Model initially does as well. Obviously we would like a much stronger proof of mass transfer by rarefaction wave dynamics, which remains an open problem relating to the global structure of the mass transfer in the full Toy Model.

6. ADDITIONAL OBSERVATIONS AND REMARKS

6.1. Flux Computation for Finite Approximations. We have the Hamiltonian system

$$(40) \quad \begin{cases} -i\partial_t b_j = -|b_j|^2 b_j + 2b_{j-1}^2 \bar{b}_j + 2b_{j+1}^2 \bar{b}_j, \\ i\partial_t \bar{b}_j = -|\bar{b}_j|^2 \bar{b}_j + 2\bar{b}_{j-1}^2 b_j + 2\bar{b}_{j+1}^2 b_j, \end{cases}$$

which is only Hamiltonian with respect to the infinite sum unless we are certain that our initial data is compactly supported. However, as suggested to us by Jonathan Mattingly [23] based off of ideas in [24], let us take initial data supported on the infinite half lattice, yet restrict the Hamiltonian system to the first N nodes and simply look at the flux in the energy at this sufficiently high node, where we now have

$$(41) \quad H_N = \sum_{j=1}^N \frac{1}{4} |b_j|^4 - \Re(\bar{b}_j^2 b_{j-1}^2),$$

which now is not perfectly conserved. Indeed, we have

$$(42) \quad \partial_t H_N = 2|b_N|^2 \Im(2b_{N+1}^2 \bar{b}_{N-1}^2 - b_{N+1}^2 \bar{b}_N^2).$$

Moving from the exact formula to do some asymptotic analysis, if we assume roughly comparable amplitude (Note: we believe is the case at say $j = \frac{N}{2}$ up to the time the rarefaction wave and dispersive shock meet) of the final three nodes gives

$$(43) \quad \partial_t H_N \approx A_N^6 [4 \sin(2\phi_{N+1} - 2\phi_{N-1}) - 2 \sin(2\phi_{N+1} - 2\phi_N)]$$

taking $b_j = A_j e^{i\phi_j}$. Hence, the Hamiltonian flux is seen to be positive (inward flow of energy) if

$$(44) \quad [\sin(2\phi_{N+1} - 2\phi_{N-1}) - \frac{1}{2} \sin(2\phi_{N+1} - 2\phi_N)] > 0.$$

In order to see outward flow of energy, the Hamiltonian flux is negative if

$$(45) \quad [\sin(2\phi_{N+1} - 2\phi_{N-1}) - \frac{1}{2} \sin(2\phi_{N+1} - 2\phi_N)] < 0.$$

For $\phi_j = \frac{(j-1)\pi}{4}$, we observe

$$(46) \quad [\sin(2\phi_{N+1} - 2\phi_{N-1}) - \frac{1}{2} \sin(2\phi_{N+1} - 2\phi_N)] = -3/2,$$

which would actually result in an outward flow of energy, though as the Hamiltonian energy is not coercive, we do not gain much from this computation.

Alternatively, we look at the restricted mass flux,

$$(47) \quad M_N = \sum_{j=1}^N |b_j|^2,$$

which now is not perfectly conserved. Indeed, we have

$$(48) \quad \partial_t M_N = -4\Im(b_{N+1}^2 \bar{b}_N^2).$$

Making a similar asymptotic assumption at the endpoint, we have

$$(49) \quad \partial_t M_N \approx -4|A_N|^4 \sin(2(\phi_{N+1} - \phi_N)).$$

Hence, we observe that the mass flux is *outgoing* for $\phi_j = \frac{(j-1)\pi}{4}$ since we then have

$$(50) \quad \partial_t M_N \approx -4|A_N|^4 \sin\left(\frac{\pi}{2}\right).$$

Remark 6.1. *As pointed out by the anonymous referee, we can use the mass flux computation from Section 6.1 to study the rarefaction wave solution from Theorem 5.1. In such a case, we observe that for say the node $j = N/2$, which remains roughly fixed at $\rho_j(t) \sim \epsilon/8$ and $\theta_j(t) \sim \pi/4$, we have the total mass moved across this node of order*

$$\epsilon^{-1}\epsilon^4 = \epsilon^3.$$

Initially, this looks like a rather small mass flux compared to the size of the solution overall. However, we note first of all that in this setting ϵ need not necessarily be extremely small since the asymptotic methods are done mostly on the side of the δ parameter. In addition, we note that numerically of course, the mid-point of the rarefaction wave solution remains stable much longer than the time scales we have controlled here. Indeed, while the rarefaction wave moving left and the dispersive shock like solution moving right definitely change the structure of the backwards Burgers equation on a time scale of order ϵ^{-1} , we have strong numerical evidence that away from the fronts of those waves the solution remains largely unchanged. Hence, we expect that with greater global control over the dynamics, the mass flux computation can be shown to be much stronger than can be applied on the time scales in Theorem 5.1.

Remark 6.2. *As commented in [9], this analysis still leads to open questions about Sobolev norm growth in the full problem (1) given the pointwise bounds on the error for $j \sim N/2$ on the same time scale, we observe that the flux computation in Section 6.1 will continue moving mass towards high j on this time scale. In addition, computational checks of the constants suggest that the bootstrapping arguments*

in Theorem 5.1 appear to go through for δ chosen even as large as $1/2$, meaning while we need our time interval to be $o(1)$, there should be parts of the argument that extend to time 1. Doing so in a rigorous fashion likely requires more analytic control on the global structure of the rarefaction wave-like solution both in discrete symmetric Burgers and in terms of the behavior in the Toy Model near the right boundary.

6.2. An observation about $\|\cdot\|_{\ell^2}$ growth of $\hat{\rho}$, $\hat{\theta}$. We present here an illustrative computation, which unfortunately at the moment we cannot apply in a perturbation theoretic argument as we would require stronger control of the behavior of solutions to (2) at the endpoints of our finite region. Let us recall that

$$\dot{\rho}_j = 4\hat{\rho}_{j-1}\tilde{\rho}_j - 4\hat{\rho}_j(\tilde{\rho}_{j+1} - \tilde{\rho}_{j-1}) - 4\hat{\rho}_{j+1}\tilde{\rho}_j + F_j,$$

with

$$F_j = 2\hat{\rho}_{j-1}\tilde{\rho}_j\tilde{\gamma}_j^2 - 2\hat{\rho}_{j+1}\tilde{\rho}_j\tilde{\gamma}_{j+1}^2 + (f)_{2,j}(t) + \mathcal{O}(|\hat{\rho}_j + \tilde{\rho}_j|^2|\hat{\theta}_j + \tilde{\gamma}_j|^2).$$

Combining terms from nearest neighbors we have

$$\begin{aligned} & \frac{1}{2}\partial_t(\hat{\rho}_{j-1}^2) + \frac{1}{2}\partial_t(\hat{\rho}_j^2) + \frac{1}{2}\partial_t(\hat{\rho}_{j+1}^2) \\ &= 4\hat{\rho}_{j-2}\hat{\rho}_{j-1}\tilde{\rho}_{j-1} - 4\hat{\rho}_{j-1}^2(\tilde{\rho}_j - \tilde{\rho}_{j-2}) - 4\hat{\rho}_j\hat{\rho}_{j-1}\tilde{\rho}_{j-1} + F_{j-1}\hat{\rho}_{j-1} \\ & \quad + 4\hat{\rho}_{j-1}\hat{\rho}_j\tilde{\rho}_j - 4\hat{\rho}_j^2(\tilde{\rho}_{j+1} - \tilde{\rho}_{j-1}) - 4\hat{\rho}_{j+1}\hat{\rho}_j\tilde{\rho}_j + F_j\hat{\rho}_j \\ & \quad + 4\hat{\rho}_j\hat{\rho}_{j+1}\tilde{\rho}_{j+1} - 4\hat{\rho}_{j+1}^2(\tilde{\rho}_{j+2} - \tilde{\rho}_j) - 4\hat{\rho}_{j+2}\hat{\rho}_{j+1}\tilde{\rho}_{j+1} + F_{j+1}\hat{\rho}_{j+1}. \end{aligned}$$

By combining nearby terms, we observe that

$$\begin{aligned} & -4\hat{\rho}_{j-1}^2(\tilde{\rho}_j - \tilde{\rho}_{j-2}) - 4\hat{\rho}_j\hat{\rho}_{j-1}\tilde{\rho}_{j-1} + 4\hat{\rho}_{j-1}\hat{\rho}_j\tilde{\rho}_j - 4\hat{\rho}_j^2(\tilde{\rho}_{j+1} - \tilde{\rho}_{j-1}) \\ & \quad - 4\hat{\rho}_{j+1}\hat{\rho}_j\tilde{\rho}_j + 4\hat{\rho}_j\hat{\rho}_{j+1}\tilde{\rho}_{j+1} - 4\hat{\rho}_{j+1}^2(\tilde{\rho}_{j+2} - \tilde{\rho}_j) \\ &= -4\hat{\rho}_{j-1}^2(\tilde{\rho}_j - \tilde{\rho}_{j-2}) + 4\hat{\rho}_j\hat{\rho}_{j-1}(\tilde{\rho}_j - \tilde{\rho}_{j-1}) - 4\hat{\rho}_j^2(\tilde{\rho}_{j+1} - \tilde{\rho}_{j-1}) \\ & \quad + 4\hat{\rho}_j\hat{\rho}_{j+1}(\tilde{\rho}_{j+1} - \tilde{\rho}_j) - 4\hat{\rho}_{j+1}^2(\tilde{\rho}_{j+2} - \tilde{\rho}_j) \\ & \leq -2\hat{\rho}_{j-1}^2(\tilde{\rho}_j - \tilde{\rho}_{j-2}) - 2\hat{\rho}_j^2(\tilde{\rho}_{j+1} - \tilde{\rho}_{j-1}) - 2\hat{\rho}_{j+1}^2(\tilde{\rho}_{j+2} - \tilde{\rho}_j) \\ & \leq 0 \end{aligned}$$

by Cauchy-Schwarz. Summation yields

$$\frac{1}{2}\partial_t \sum_{j=1}^N \hat{\rho}_j^2 \leq 2\hat{\rho}_N^2(\tilde{\rho}_N + \tilde{\rho}_{N-1}) + \sum_{j=1}^N F_j \hat{\rho}_j$$

since the $\hat{\rho}$ terms are compactly supported on the interval $j = 1, \dots, N$. Hence, we observe that on the time scale of evolution, the leading order terms here involve only the right endpoints and are by construction positive, which fits with the conservation of mass in (2).

6.3. Other Discrete Conservation Laws. In [20], the authors study Fermi-Pasta-Ulam Systems of the form

$$\dot{r}_j = v_{j+1} - v_j, \dot{v}_j = \phi'(r_j) - \phi'(r_{j-1}),$$

where $\phi(r) = e^{1-r} - (1-r)$. Continuous limits $(r_j, v_j)(t) = (r, v)(\epsilon t, \epsilon j)$ of such models also satisfy the Burgers equation

$$\partial_t r - \partial_x v = 0, \quad \partial_t v - \partial_x \phi'(r) = 0.$$

Rarefaction waves and dispersive shocks are observed and studied in depth numerically and some analysis is done on conservative shock formation. In future work, we hope similar analysis can be done to that for (2).

7. NUMERICAL STUDY OF RAREFACTION AND RELATIONSHIP TO THE TODA LATTICE

Following a suggestion of the referee, the authors explored references [12, 11, 21] relating symmetric Burgers (8) and the Toda Lattice, a known integrable system, see also the survey article [26]. The key idea is that $\sqrt{\rho_j}(t/4) = a_j(t)$, the system becomes the Kac-van Moerbeke system (KvM)

$$(51) \quad \dot{a}_j = -a_j(a_{j+1}^2 - a_{j-1}^2)$$

and this has a direct connection via its even and odd modes to the Toda Lattice by interpreting the a_j 's as entries in a Jacobi Matrix. In [11], they construct the algebro-geometric inverse of the Toda Solitons to the KvM system, which translates in discrete Burgers to solutions on all of \mathbb{Z} of the form

$$(52) \quad \rho_j(z, t) = \gamma \begin{cases} \frac{1+c(t)^2 z^{2m+2} (1-z^2)^{-1}}{2z(1+c(t)^2 z^{2m} (1-z^2)^{-1})}, & j = 2m, \\ \frac{z(1+c(t)^2 z^{2m} (1-z^2)^{-1})}{2(1+c(t)^2 z^{2m+2} (1-z^2)^{-1})}, & j = 2m + 1, \end{cases}$$

where

$$c(t) = c_0 e^{\frac{(z-z^{-1})t}{2}},$$

where the constant γ determines the total amplitude and partially the time of evolution compared to the (KvM) system. The rarefaction wave can be seen as the setting where $z = 1$. Otherwise, this solution gives interesting splitting of the even and odd modes that we will show remains somewhat stable in the toy model.

First, we numerically have studied the evolution of out of phase initial data with amplitude given by the mapped 1-soliton solution wave truncated to a domain of 400 nodes with $\gamma = .1$, $z = .1$ and $c_0 = 1.0$ in Figure 3. As one can observe, there are some interesting features in the Toy Model as well as in the Burgers solution, but backward

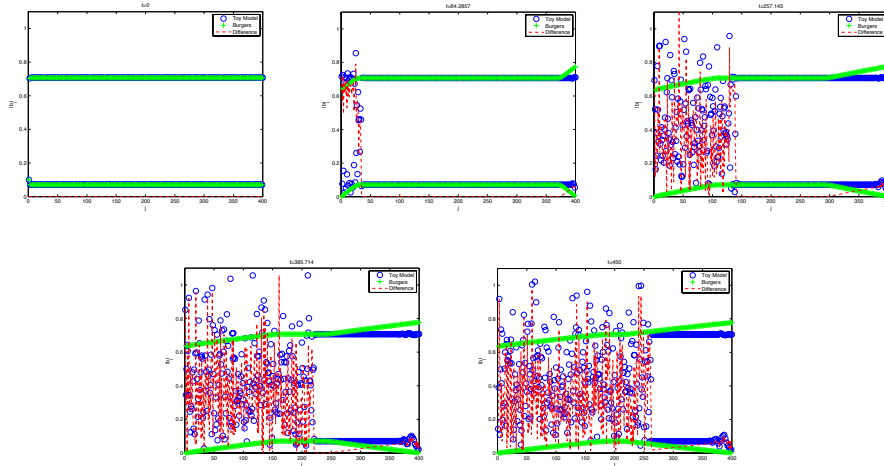


FIGURE 3. A comparison of the evolution of solutions stemming from an initial amplitude profile given by a truncated Toda soliton solution with parameters $\gamma = .1$, $z = .1$ and $c_0 = 1.0$.

propagation from the truncation on the right and drag in the phase cause the solution to differ significantly on a similar time scale to the rarefaction wave.

However, based upon the insight that the Toda lattice soliton can generate mass exchange, in Figure 4, we then took out of phase initial data corresponding to (52) on the first $M = 4$ nodes, then continued by $\rho_j = z/2$ for $j > M$. Interestingly enough, this initial data generates right traveling nodes at fast time scales in the Burgers model and as seen in Figure 4 seems to lead to a slow, but steady oscillating traveling wave in the Toy Model. The peaked wave observed there persists on longer domains and with decaying tails to the right (provided the decay is slow). Also, a peaked wave of this form can be observed choosing M as small as 6, but there does not appear to be enough energy if $M = 2$ or 4. The dynamics are generally on a much slower scale than that of the comparable symmetric Burgers equation, but the traveling wave observed is rather intriguing as a potential for mass transfer.

Lastly, in Figure 5, we studied the evolution of a simple out of phase rarefaction wave on $N = 2000$ nodes with $\rho_j = 1$ on the first $M = 100$ nodes, then a decaying tail of the form $\rho_j = 1/(1 + .1(j - 100)^{1/2})$ for $j > 100$. The general flow of the mass can be seen to be to the right, though of course in such a setting we have no envelope equation with which to try to approximate the dynamics.

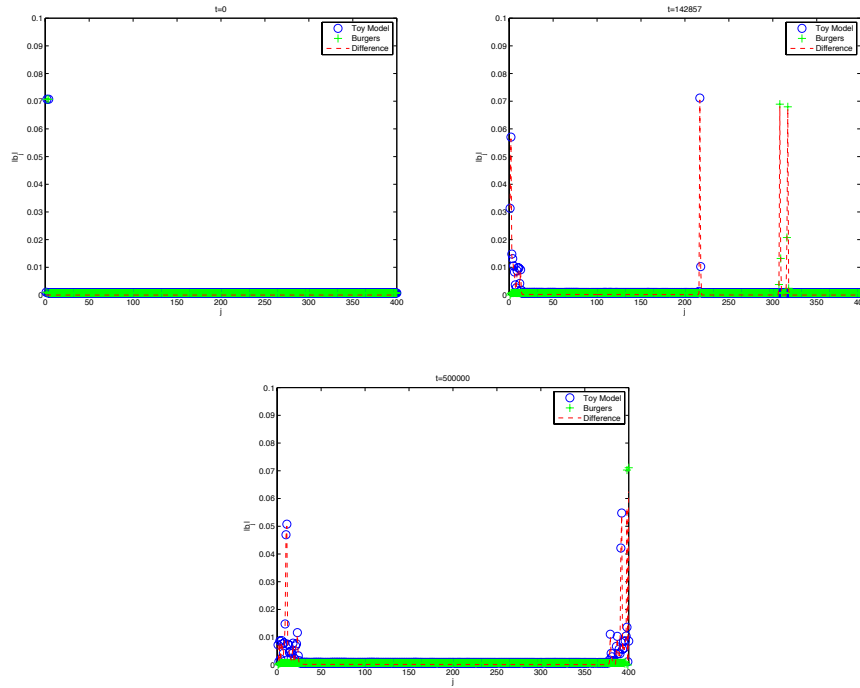


FIGURE 4. A comparison of the evolution of solutions stemming from an initial amplitude profile given by applying the Toda soliton solution on an even number of nodes at the left, then continuing on the right as a small non-zero constant with parameters $\gamma = .0001$, $z = .01$ and $c_0 = 1.0$.

Acknowledgements. The first author was supported by the German Research Foundation, CRC 701. The second author was supported by a combination of an IBM Junior Faculty Development Award through the University of North Carolina, NSF Grant 1312874, plus Guest Lectureships through Universität Bielefeld Summer 2012 and Karlsruhe Institute of Technology in Summer 2013.

Thanks especially to Gideon Simpson for many helpful conversations about this topic and for allowing us to modify his code to create the pictures seen here. The authors also wish to thank Jianfeng Lu, Hiro Oh and Jonathan Mattingly for interesting discussions, but particularly Mattingly for suggesting the flux computation displayed in Section 6.1. In addition, the authors thank the anonymous referees for pointing out many places the exposition could be improved or clarified and in

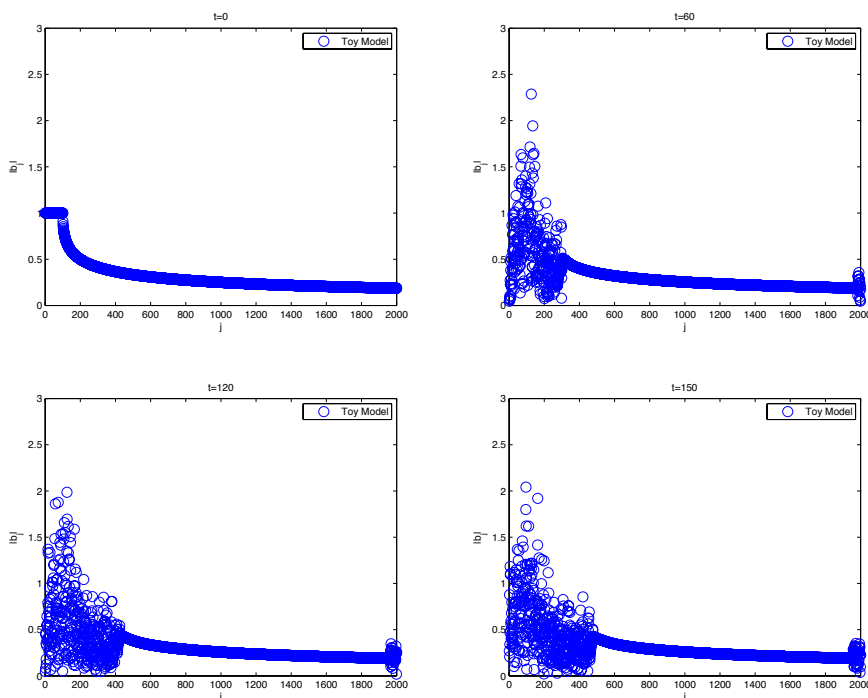


FIGURE 5. A comparison of the evolution of solutions for a rarefaction wave profile with a decaying tail of form $1/(1 + .1 * j^{\frac{1}{2}})$ to minimize the backward propagating shock from the right boundary.

particular for such a careful reading of the article. Also, for pointing out the connection to the Toda Lattice, which proved invaluable.

REFERENCES

- [1] E. Ben-Naim and P. Krapivsky. Discrete Analog of the Burgers Equation. Preprint, arXiv:1209.0043.
- [2] E. Ben-Naim and S. Redner. Dynamics of Social Diversity. *J. Stat. Mech. Theory Exp.*, (L11002), 2005.
- [3] J. Bourgain. Aspects of long time behaviour of solutions of nonlinear hamiltonian evolution equations. In *Geometries in Interaction*, pages 105–140. Springer, 1995.
- [4] J. Bourgain. On the Cauchy problem for periodic KdV-type equations. *Journal of Fourier Analysis and Applications*, 1:17–86, 1995.
- [5] J. Bourgain. On the growth in time of higher Sobolev norms of smooth solutions of Hamiltonian PDE. *International Mathematics Research Notices*, 1996(6):277–304, 1996.

- [6] J. Bourgain. Remarks on stability and diffusion in high-dimensional Hamiltonian systems and partial differential equations. *Ergodic Theory Dynam. Systems*, 24(5):1331–1357, June 2004.
- [7] R. Carles and E. Faou. Energy cascades for NLS on the torus. *Discrete and Continuous Dynamical Systems. Series A*, 32(6):2063–2077, 2012.
- [8] J. Colliander, M. Keel, G. Staffilani, H. Takaoka, and T. Tao. Transfer of energy to high frequencies in the cubic defocusing nonlinear Schrödinger equation. *Inv. Math.*, 181(1):39–113, 2012.
- [9] J. E. Colliander, J. L. Marzuola, T. Oh, and G. Simpson. Behavior of a model dynamical system with applications to weak turbulence. *Exp. Math.*, 22(3):250–264, 2013.
- [10] E. Faou, P. Germain, and Z. Hani. The weakly nonlinear large box limit of the 2D cubic nonlinear Schrödinger equation. Preprint, arXiv:1308.6267.
- [11] F. Gesztesy, H. Holden, B. Simon, and Z. Zhao. On the Toda and Kac-van Moerbeke systems. *Trans. Amer. Math. Soc.*, 339(2):849–868, 1993.
- [12] J. Goodman and P. D. Lax. On dispersive difference schemes. I. *Comm. Pure Appl. Math.*, 41(5):591–613, 1988.
- [13] B. Grébert, É. Paturel, and L. Thomann. Beating effects in cubic Schrödinger systems and growth of Sobolev norms. Preprint, arXiv:1208.5680.
- [14] B. Grébert and L. Thomann. Resonant dynamics for the quintic nonlinear Schrödinger equation. *Ann. Inst. H. Poincaré Anal. Non Linéaire*, 29(3):455–477, 2012.
- [15] M. Guardia. Growth of Sobolev norms in the cubic defocusing nonlinear Schrödinger equation with a convolution potential. Preprint arXiv:1211.1267.
- [16] M. Guardia and V. Kaloshin. Growth of Sobolev norms in the cubic defocusing nonlinear Schrödinger equation. Preprint, arXiv:1205.5188 (to appear in *J. Eur. Math. Soc.*).
- [17] Z. Hani. Long-time instability and unbounded Sobolev orbits for some periodic nonlinear Schrödinger equations. Preprint, arXiv:1210.7509, 2012.
- [18] Z. Hani, B. Pausader, N. Tzvetkov, and N. Visciglia. Modified scattering for the cubic Schrödinger equation on product spaces and applications.
- [19] E. Haus and L. Thomann. Dynamics on resonant clusters for the quintic nonlinear Schrödinger equation. Preprint arXiv:1210.7291.
- [20] M. Herrmann and J. D. Rademacher. Riemann solvers and undercompressive shocks of convex fpu chains. *Nonlinearity*, 23:277–303, 2010.
- [21] M. Kac and P. van Moerbeke. On an explicitly soluble system of nonlinear differential equations related to certain Toda lattices. *Advances in Math.*, 16:160–169, 1975.
- [22] S. Kuksin. Oscillations in space-periodic nonlinear Schrödinger equations. *Geom. Func. Anal.*, 7(2):338–363, 1997.
- [23] J. Mattingly. Personal Communication, 2012.
- [24] J. C. Mattingly, T. Suidan, and E. Vanden-Eijnden. Simple systems with anomalous dissipation and energy cascade. *Comm. Math. Phys.*, 276(1):189–220, 2007.
- [25] V. Sohinger. Bounds on the growth of high Sobolev norms of solutions to nonlinear Schrödinger equations on S^1 . *Differential Integral Equations*, 24(7-8):653–718, 2011.

- [26] G. Teschl. Almost everything you always wanted to know about the toda equation. 2001.

UNIVERSITÄT BIELEFELD, FAKULTÄT FÜR MATHEMATIK, POSTFACH 10 01 31,
33501 BIELEFELD, GERMANY

E-mail address: `herr@math.uni-bielefeld.de`

MATHEMATICS DEPARTMENT, UNIVERSITY OF NORTH CAROLINA - CHAPEL
HILL, CHAPEL HILL, NC 27599, USA

E-mail address: `marzuola@math.unc.edu`